Journal of Agricultural Engineering

ArduHydro: a low-cost device for water level measurement and monitoring

Andrea Galli, Cosimo Peruzzi, Fabiola Gangi, Daniele Masseroni

Publisher's Disclaimer

ArduHydro: a low-cost device for water level measurement and monitoring

Andrea Galli,[1,2] Cosimo Peruzzi,[1,3] Fabiola Gangi,[1] Daniele Masseroni[1]

[1]Department of Agricultural and Environmental Sciences (DiSAA), University of Milan; [2]Ca' Granda Heritage Foundation, Milan; [3]Italian Institute for Environmental Protection and Research (ISPRA), Area for Hydrology, Hydrodynamics, Hydromorphology and Freshwater Ecology (BIO-ACAS), Rome, Italy

Correspondence: Andrea Galli, Department of Agricultural and Environmental Sciences (DiSAA), University of Milan, Via Celoria 2, 20133 Milan, Italy.
E-mail: andrea.galli@fondazionepatrimoniocagranda.it

Key words: low-cost sensor; water level; Arduino; monitoring; irrigation.

Conflict of interest: the authors declare no potential conflict of interest.

Availability of data and materials: all the data used in this study are available, upon request, by contacting the corresponding author.

Abstract

In this paper, we present ArduHydro, a low-cost device for water level measurement and monitoring designed for employment in controlled and outdoor environments. It measures the water level through an ultrasonic sensor and elaborates the signals through an Arduino microcontroller. The small size of this device, its robustness and accuracy make ArduHydro properly versatile for different applications in the field of water control and management. This article describes the design, the components, the costs, and the performance of ArduHydro. The performance was assessed with a laboratory test inside an open-channel flume and comparing ArduHydro measurements with those obtained with a traditional ultrasonic sensor. Furthermore, an example of ArduHydro application for detecting the wavefront evolution during surface irrigation of a maize crop is presented. The results revealed that ArduHydro measurements were, on average, very consistent with those obtained by the traditional ultrasonic sensor in all different flow conditions. The application of ArduHydro during a surface watering of an agricultural field allowed us to obtain important spatiotemporal information about the water depth along the longitudinal direction of the field, paying the way for a real comprehension of the dynamics of wavefront evolution in a real-world case study.

Introduction

The acquisition of on-field ~~data~~ information is a crucial task in many research areas and, over time, the necessity to gather data with ever higher spatial and temporal resolutions is emerging (Montanari et al., 2013). In recent years, and particularly in environmental sciences, this hunger for data has found a significant help in the so-called low-cost monitoring systems (Mao et al., 2019; Tauro et al., 2018; Toran, 2016; Tscheikner-Gratl et al., 2019; Wickert et al., 2019). Considering the definition provided by (Cherqui et al., 2020), the jargon *low-cost technology* refers to systems that have a substantially lower price than traditional/commercial technology. The reasons to use low-cost monitoring systems are numerous and not only linked to affordability: for instance, these technologies are also fully customizable, open-source, and allow users not to rely on proprietary technologies developed by a specific commercial company (Fisher and Gould, 2012; Mao et al., 2019). For the abovementioned reasons, the research for novel low-cost technologies that are more versatile and cheaper in comparison to commercial equipment ~~is~~ has been a trending topic in recent years (Fisher et al., 2020). Undoubtedly, the growing attention to ~~realization of~~ low-cost hand-made devices is favoured ~~possible only~~ thanks to the development of low-cost microcontrollers like Arduino, Beagleboard, or Raspberry (Harnett, 2011; Pearce, 2012), the advancement in additive manufacturing

(Baden et al., 2015) and the rapid advances in electronic technologies that have led the availability of sensors and auxiliary components at affordable prices (Fisher and Gould, 2012; Mao et al., 2019).

In this sense, the agricultural engineering field was particularly fruitful and, over the years, very diversified low-cost self-made devices with different applications have been proposed. Just to recall some of them, Facchi et al. (2017) presented a device for the measurement of soil evaporation in aerobic rice fields, Masseroni et al. (2016) proposed an open-hardware tool for the continuous monitoring of soil water potential in the root zone, Ravazzani (2017) developed a portable probe for the quantification of the soil moisture, while Chiaradia et al. (2015) realized a multisensory system for the continuous monitoring of water dynamic in rice fields.

One of the most important hydraulic parameters to evaluate and control is the free-surface water level, which can be useful for several applications, such as water flow management, prediction of flood and drought, water quality assessment, irrigation, and smart agriculture (Errico et al., 2019; Illes et al., 2013; Loizou and Koutroulis, 2016; Peruzzi et al., 2021a; Tscheikner-Gratl et al., 2019; Vijay Hari Ram et al., 2015). Considering the hydraulic engineering sector, there are a plethora of commercial instrumentations devoted to this goal, i.e. staff gauges, electric-tape gauges, float-tape gauges, pressure transducers, or acoustic transducers (Herschy, 2009). However, these traditional instruments generally are placed in a dedicated fixed installation, and therefore they are impractical to be transported in different in-situ locations, as it happens instead in the most common agricultural applications. Moreover, traditional instrumentations might not have a justifiable cost in some circumstances or applications (e.g. in farming). Hence, in the last decade, different in-situ devices for water level measurements have been proposed, based on video surveillance (Noto et al., 2021; Schoener, 2018; Zhang et al., 2019), low-cost sensors (Ezenne and Okoro, 2019; Hund et al., 2016; Kabi et al., 2023; Loizou et al., 2015; Rosolem et al., 2013), low-cost GNSS antenna arrays (Karegar et al., 2022; Purnell et al., 2021) and unmanned aerial vehicle (Gao et al., 2019; Ichikawa et al., 2019). Nevertheless, it is not so common to find low-cost devices that are also robust, easy to transport, install and disassemble and, at the same time, sufficiently accurate. With this purpose in mind, we present ArduHydro, a low-cost self-made open-access device for the monitoring of water levels that is a compact, robust, and very versatile instrument that can be installed in different ways on-site and easily removed to download the data. Another strong point of the ArduHydro sensor lies in the fact that, being inexpensive, several of them can be built and deployed simultaneously in the study area, gathering data at a high spatial frequency.

This work is composed as follows: after this brief introduction, Section 2 describes in great detail how ArduHydro is composed and its functioning (Section 2.1), the open-channel flume facility used

to assess the quality of the measurements (Section 2.2), and the agricultural field in which an example of field application is presented (Section 2.3). Section 3 is dedicated to showing and discussing the methodology for the data processing and then the output from the laboratory (Section 3.1) and in-field (Section 3.2) measurements. Finally, Section 4 summarizes the main outcomes.

Material and Methods

The ArduHydro device

The idea underpinning ArduHydro is to have a compact and versatile tool to monitor the water depth in different contexts. The sensor chosen to obtain the measurement is an ultrasonic range finder. To now, this type of sensor presents the best performance-to-price ratio on the market (Cherqui et al., 2020) and they are widely used in many applications with the most disparate purposes. Starting from the Arduino Tutorial[1] indications, we have created a customised product that can satisfy both the needs of measurement accuracy and transport versatility. To fulfil this goal, we made major improvements to the device shown in the tutorial, such as the employment of a more accurate sensor, correction of measurements based on air temperature, internal data logging and data filtering. In the following, all the information about the hardware, the software program, the specifications of the sensors, and the cost of the components are described in detail.

Microcontroller board

The microcontroller board is based on the open-source *Arduino Nano* system and consists of a microcontroller (MCU) equipped with a bootloader for programming, a built-in support for serial communication (FTDI chip), and other complementary components such as a power supply regulator, Mini-USB connector, digital and analogue pins for interfacing with external devices (e.g. sensors). The board can be powered with an unregulated power supply via the "Vin" pin (7 – 12V), with a regulated 5V power supply via the "5V" pin, or using the mini-USB connector (5V). The MCU is an ATmega328P microcontroller (Atmel Corporation, San Jose, Calif., USA) that features 14 digital ports and 6 analogue ports, which can be used as inputs (e.g. for sensor reading) or outputs, with an operating voltage of 0 – 5V. The ATmega328P operates at a frequency of 16mHz and has 32 KB of flash memory, which serves as storage for the main operating program, as well as 1 KB EEPROM. The writing, compiling, and uploading of a program to the MCU can be easily carried out using an open-source integrated development environment (IDE)[2].

---

[1] https://arduinogetstarted.com/tutorials/arduino-ultrasonic-sensor
[2] freely downloadable at http://www.arduino.cc

Power supply

The board is powered using a 9V Li-ion battery with a total capacity of 650mAh and is used in turn to power all external modules and sensors through the "3.3V" and "5V" pins as shown in Figure 1. The battery has a Micro-USB socket for quick and convenient recharging via USB cable. When the device is not in use, the power supply can be interrupted using a simple SPST switch. The average power consumption of the device is around 25 mA, which means the theoretical battery life is 26 hours of continuous usage.

Sensors

As shown in Figure 1, the microcontroller board is connected to two sensors: an ultrasonic range finder and a digital thermometer.

The ultrasonic range finder is an HY-SRF05 model, with a supply voltage of 4.5 – 5.5V and a digital pin interface. The sensor, working as both an ultrasound transmitter and receiver, can be used to measure distance in a range between 0.02 and 4.5 m with resolution up to 0.2 cm, has a maximum sampling frequency equal to 40 Hz, and a detection angle of 15°.

The digital thermometer is a DS18B20 sensor, with a 3-5.5V supply voltage, 1 wire bus interface, measuring range from -55 °C to +125 °C, $\pm$0.5°C accuracy, and resolution up to 0.0625 °C. The sensor is contained in a waterproof stainless-steel enclosure.

Data logging

To allow long-term storage of measured data, the device is equipped with a MicroSD card reader module. The module can be used to transfer data to an external memory cartridge (MicroSD) via an SPI interface. The voltage needed to power the MicroSD reader is between 4.5 and 5.5 V. Due to the nature of the collected data, consisting of small-size text files, relatively low-profile storage cards are sufficient. For our purposes, a 256 Mb card was used for data logging.

A DS3231 Real-Time-Clock (RTC) module was added to the device for data logging. This module features an integrated temperature-compensated crystal oscillator (TCXO) for higher accuracy. The RTC is supplied with a voltage of 5 V by the microcontroller board when the device is switched on, and by a CR2032 backup battery when the device is switched off.

Enclosure

All electronic components are fitted in a 100X100X50 mm plastic enclosure with IP56 protection, which protects against impacts and weather. The two sensors are positioned in the lower part of the enclosure, with the ultrasound transmitter/receiver of the HY-SRF05 and the waterproof probe section of the DS18B20 being the only parts exposed (Figure 2a). The main switch is mounted on the upper part of the enclosure (with a silicone cover for waterproofing), alongside a small bubble level which facilitates the correct positioning of the device (Figure 2b). This configuration allows ArduHydro to operate in unfavourable weather conditions with minimal risks of damage to the electronic components.

Costs

The cost of each component used for building an ArduHydro device is shown in Table 1. The price shown under the Cost column refers to the purchase of a single component. For this study, ten ArduHydros were built, reducing the cost of individual components through batch purchases. The batch cost for each component is shown in the Batch cost column.

Operating principle

When measuring water levels, ArduHydro is mounted 2 - 450 cm above the water with the lower part directly facing the water surface and parallel to it. The distance between the sensor and the ground is then manually measured employing a graduate rod (precision ± 1 mm) and noted down. Once the device is switched on, the microcontroller board controls the operation of each component according to a program, called "sketch", which was uploaded to the MCU via Arduino IDE and USB serial interface, as explained in Section 2.1.1. The sketch consists of two parts: "setup" and "loop". The setup mainly consists of the initialization of libraries (packages with built-in functions) and the declaration of variables and is only executed once after the device is powered (this usually takes a few seconds), whereas the loop contains the main operating functions of the device, and is repeatedly executed in its entire length until the device is powered off. During the initial setup, a .txt file is created on the MicroSD to use for permanent storage of acquired data. The first operation carried out by ArduHydro in the loop segment of the sketch is temperature measurement via the DS18B20 sensor. This parameter is used to calculate the speed of sound in air (Wong and Embleton, 1985) as shown in Eq.(1):

$$c = \sqrt{\frac{\gamma R T}{M}} \qquad (1)$$

8

where c (m/s) is the speed of sound, γ is the specific heat ratio, R (j/(mol*K)) is the universal gas constant, T (K) is the absolute temperature, and M (kg/mol) is the molar mass of air. Since $\gamma = 1.4$, $R = 8.3145$ J/K mol, and $M = 0.028966$ kg/mol (Hilsenrath et al., 1955), Eq.(1) becomes:

$$c = 20.05\sqrt{T} \tag{2}$$

Subsequently, the MCU sends a 10 µs HIGH signal at the Trigger pin (Trig) of the HY-SRF05 sensor. This prompts the ultrasonic transducer to emit a 40 kHz ultrasonic wave. If the wave encounters the water surface (or any other solid obstacle), it is reflected toward the sensor's receiver. Once the return wave is detected, the sensor returns the value of the time elapsed since the emission of the wave (time of flight), which is then used to calculate the distance between the sensor and the water as follows:

$$d = \frac{ct}{2} \tag{3}$$

where d (m) is the distance and t (s) is the time of flight. Lastly, a string variable consisting of the date and time, t and d (separated by commas) is created and printed on a new line of the .txt file on the MicroSD. The loop segment is then repeated until the device is powered off, with each cycle lasting 0.2 seconds. This means that ArduHydro has a measuring frequency of 5 Hz. Once data is retrieved from the MicroSD card, the values of distance from the water surface can be used to calculate the water level as shown in Eq.(4):

$$h = L - d \tag{4}$$

where h (m) is the water depth and L (m) is the distance between the sensor and the ground. In case the device is permanently mounted at a fixed position, this last procedure can be integrated within the sketch to directly record the water depth values in the datalog file. However, this was not the case in the context of our study.

Laboratory experimental set-up

To quantify the performance of ArduHydro (AH) devices in measuring water levels, we have conducted a series of experiments aimed to test the devices in different hydraulic conditions. The experiments were carried out in a non-tilting, recirculating, open-channel flume at the Hydraulics Laboratory of the University of Pavia (Figure 3a-b). Furthermore, Figure 3a reports the origin of the axes coordinate system used in the present study (i.e. the longitudinal x and vertical y directions). The main part of the facility is composed of a rectangular channel, which is 8.50 m long, 0.49 m wide, and 0.75 m deep. The flume has transparent Polymethyl methacrylate (PMMA) sidewalls and a metallic bed. The water levels h inside the flume are regulated through a vertical sluice gate placed at the end of the facility. The incoming flow rate Q, controlled by the presence of a gate valve in the

delivery pipe, is measured upstream of the main part of the flume by means of a triangular-notch Thomson weir using (Shen, 1981):

$$Q = C \frac{8}{15} \sqrt{2g} \tan\left(\frac{\theta}{2}\right) h_w^{5/2} \tag{5}$$

where C is the non-dimensional coefficient of discharge, g is the acceleration due to gravity, θ is the angle between the two sides of the notch (expressed in degrees) and h_w is the upstream piezometric head measured with respect to the vertex of the notch. For this specific weir, C and θ are equal to 0.72 and 36°, respectively. The piezometric head h_w is ~~estimated~~ measured with the aid of a manual piezometer equipped with a sharp point gauge connected to a vernier calliper (accuracy of 0.05 mm) placed in proximity to the triangular-notch Thomson weir. The distance between the channel bottom and the vertex of the notch is 0.152 m. A dissipation basin realized with a series of holed concrete blocks is placed downstream of the falling water coming from the weir to reduce the energy and turbulence of the flow approaching the inlet of the flume (Figure 3a). During some tests, a floating breakwater device realized in polystyrene was used to further reduce the free-water surface oscillations.

The position of the three AH devices involved in the experiments is shown in Figure 3a-b together with the displacement of the four ultrasonic (US) distance sensors (PIL Sensoren GmbH, model: P43-F4V-2D-1C0-220E) used as a benchmark. Indeed, ultrasonic distance sensors are widely used in laboratory applications concerning flows with a free surface and represent the standard in many situations (e.g. Marino et al., 2018; Peruzzi et al., 2020, 2021b; Zhang et al., 2018). The used USs (sampling frequency of 400 Hz) have a nominal accuracy of ± 1 mm that remains constant if the US works within its optimal sensing distance (i.e. between 8 and 160 cm away from the sensor). The ultrasonic signal emitted by the US propagates with a divergence angle equal to 8°. Another manual piezometer was placed close to the third US (Figure 3a-b) and used to have a further comparison.

In Section 3.1, the comparison between the AH sensor and the US sensor is made considering those in position 2 and in position 3 (Figure 3a), where a distance of 20 cm in the x direction between them was set. This distance is relatively low, hence possible differences between the water levels measured by the HA sensor (h_{AH}) and by the US sensor (h_{US}) due to hydraulic losses of the flow fall within the instrumental uncertainties. Furthermore, this distance ensures that the ultrasonic beams of the two sensors do not overlap.

Experimental procedure and hydraulic conditions

The water depths were measured during the entire duration of the six experiments listed in Table 2 by both the three AH and the four US sensors placed along the flume (Figure 3a). All the sensors were turned on simultaneously and, after that, the gate valve was opened in order to reach the desired flow rate. In this way, the water stages were recorded in rather different moments, i.e., from the passage of the first wavefront to the establishment of the steady-state condition within the channel. The onset of the steady-state condition occurred when the water levels remain constant (within a range of ±1.5 mm) at the downstream piezometer section. During the steady-state condition, the water depth at the downstream manual piezometer h_p and the bulk velocity U_b were ~~estimated~~ measured and calculated, respectively, to characterize each experiment.

Exp 4 to 6 were conducted with the aid of the floating breakwater device in order to reduce the oscillation of the free surface.

Field experimental set-up

In addition to the laboratory test, an experiment in an outdoor environment was carried out to evaluate the performance of the ArduHydro device for the detection of the waterfront advance (wavefront) during surface irrigation. In particular, an agricultural field sowed with maize and located in the province of Mantua (Italy), whose details can be found in Masseroni et al. (2021, 2022), was considered as a case study (Figure 4). The field is about 1.5 ha in size, divided into 4 borders, three of which have a quasi-rectangular shape of approximately 30 m in width and ~~approximately 100~~ 120 m in length. The slope is about 0.61%, with a regular longitudinal profile, which was determined through a photogrammetric drone flight (Costabile et al., 2023). Closed-end border irrigation is the method for watering each border. Specifically, borders are irrigated by diverting a stream of water from the channel to the upper end of the border (points P1-4 in Figure 4). The water flows down the slope and when the desired amount of water has been delivered to the border, the stream is turned off. Ten AH sensors were installed along the longitudinal direction of the border (starting from the inlet point of the irrigation flow rate) for detecting spatiotemporal wavefront evolution. The AHs' field placement consisted of simply inserting part of the metal rod on which they were mounted directly into the soil (Figure 4). The distance from the inlet of each sensor and its elevation from the ground are reported in Table 3. The elevation, useful for achieving water depth through Eq.(4), was measured manually using a graduated rod (precision ±1 mm), while a thin wooden board was inserted at the base of each post to have a uniform level of the ground under the sensor (Figure 4). All sensors were switched on at the same time and the irrigation began exactly 11 minutes and 55 seconds after they switched on.

The selected irrigation event was carried out on July 20, 2021. It was characterized by a flow rate of 367.4 l/s supplied for the examined border (i.e. border 2) for 48 minutes.

Results and Discussion

Results from the laboratory campaign

Before comparing the measurements performed by AHs with those carried out by US devices, two data filtering methods were employed to eliminate artefacts and outliers from collected AH raw data. At first, a simple data range filter was used, removing all negative values and all measurements exceeding the manually measured distance from the open-channel flume's bed. The second procedure was used to remove all errors attributable to delayed signals caused by uneven reflection on the water surface, which resulted in longer measured distances and consequently lower water levels. This involved calculating the moving maximum with a range of 10 measurements (2 seconds) and removing all data being more than 10% lower than this value. An example of the results achieved by the application of the two filtering methods is shown in Figure 5, where AH raw and processed data are compared with US measurements.

Once the best methodology for processing ArduHydro's output data was found, this procedure was then applied to all the acquired water level signals. Figure 6 shows the evolution of the water levels during each laboratory experiment. It can be noted a good agreement between the water levels measured by the US and AH sensors. As expected, Exps 1-3 (Figure 6a-c) show a higher fluctuation of the free surface concerning the other tests (Exps 4-6, Figure 6d-e), where a floating breakwater device was inserted. In this way, it was possible to assess the performance of the AH sensors in different free surface flow conditions. In general, the US seems to be more accurate ~~to catch~~ in catching the small fluctuations of the free surface and this can be explained by the fact that the instrument measures by averaging the free surface fluctuations in a smaller area with respect to the AH sensors. Indeed, depending on the experimental conditions (Table 2), the water level datum is inferred over an area of $76.30 – 106.26$ cm^2 with the USs against an area of $215.55 – 311.35$ cm^2 by using the Ahs due to the different sensors' detection angles.

Furthermore, it can be seen from Figure 6 how an unsteady phenomenon starts to occur in the first minutes of each Exp (hereinafter referred to as 'transient flow'). Specifically, a hydraulic jump takes place that moves from the downstream end of the flume to the upstream end due to the obstruction caused by the presence of the sluice gate. In the following, although this transient flow is well described also by the AH sensors, we omit to quantitatively compare the US and AH measurements during the passage of this unsteady flow since the distance of 20 cm in the longitudinal direction

between the US and AH sensors (see the discussion in Section 2.2) become relevant and hence it can induce misinterpretation of the data.

To better understand the performance of the AH sensors, Figure *7* 7 reports the measured water levels by the two types of sensors in a scatter plot diagram. The data used for the comparison are only those that were recorded exactly at the same time by both sensors in positions 2 and 3 in the flume (Figure 3a). From these scatter plots, we can throw down the following indications: the AH sensors deliver a similar quality of information (i) as long as the free surface becomes smoothers and (ii) as long as the distance between the free surface and the AH sensor decreases. For what concerns the first statement, it is evident a less scatter in the data by comparing, for instance, Figure 7a with Figure 7d. Considering the second statement, the AHs performance strongly increases from Exp 1 to Exp 3 (Figure 7a and Figure 7c), where the distance between the sensor and the water is reduced by about 15 cm. Thus, although the sensor mounted in the AH works with a wide range of distances ($2 - 450$ cm as reported by the manufacturer, see Section 2.1.3), to properly measure water levels, the optimal distance seems to be around 55 cm from the free surface.

Table 4 shows the results given by some quantitative statistical indicators used to further characterize the AHs performance, i.e. the Pearson correlation coefficient r, the coefficient of determination R^2 and the root-mean-square error $RMSE$ that are defined as (Dawson et al., 2007):

$$r = \frac{1}{N-1} \sum_{i=1}^{N} \left(\frac{h_{AH_i} - \mu_{h_{AH}}}{\sigma_{h_{AH}}} \right) \left(\frac{h_{US_i} - \mu_{h_{US}}}{\sigma_{h_{US}}} \right) \tag{6}$$

$$R^2 = 1 - \frac{\sum_{i=1}^{N} \left(h_{US_i} - h_{AH_i} \right)^2}{\sum_{i=1}^{N} \left(h_{US_i} - \mu_{h_{US}} \right)^2} \tag{7}$$

$$RMSE = \sqrt{\frac{1}{N} \sum_{i=1}^{N} \left(h_{US_i} - h_{AH_i} \right)^2} \tag{8}$$

where $\mu_{h_{AH}}$ and $\sigma_{h_{AH}}$ are the mean and standard deviation of h_{AH}, respectively, and $\mu_{h_{US}}$ and $\sigma_{h_{US}}$ are the mean and standard deviation of h_{US}, while N is the size of the dataset. Eqs (6) - (8) were computed considering the dataset shown in Figure 7 without the transient flow (grey dots).

From Table 4 we can see that the comparison between AH and US sensors in position 2 and position 3 gives pretty much the same outcome, showing that the results are independent of the spatial position along the flume. As already noted in Figure 7, Exp 1 shows the worst scenario, where the free surface has the biggest fluctuations and the greatest distance from the sensor. In this situation, R^2 is rather low, giving a mean value of 0.6 and a root-mean-square percentage error, i.e. $100 \cdot \left(RMSE/\mu_{h_{US}} \right)$,

equal to 7.7%. Instead, considering Exp 2 and Exp 3 which are also characterized by a free surface not smoothed by the presence of the floating device, they reveal a very good R^2 (Table 4). ~~On the opposite side, all the other Exps~~ In general, Exps from 2 to 6 show an $R^2 > 0.91$ with a root-mean-square percentage error in the range 2.9 - 6%, depending on the ~~test~~ experiment.

Results from the field campaign

In this section, we present a potential application of the ArduHydro sensors in the agricultural water management ~~field~~ context. As pointed out by Masseroni et al. (2017), surface irrigation practices, still largely adopted in the world for watering row crops, cannot be completely replaced by modern pressure systems since they give positive externalities in terms of ecosystem services to the surrounding environment and landscape. However, increasing the efficiency of surface irrigations (such as border irrigation) is desirable and needed in light of the effects that climate change is having on the availability of water resources for irrigation (Chen et al., 2013; Masseroni et al., 2022).

In this scenario, AH sensors can be involved as an advantageous tool to measure the water levels within a crop field and hence to quantitatively characterize the irrigation, both from a spatial and temporal point of view. That information can then be used to calibrate and validate models useful to guide the decision-makers to establish scientific-based guidelines for the farmers (Costabile et al., 2023).

As an example, here we report the evolution in time of the irrigation wavefront (Figure 8) measured during a border irrigation event on July 20, 2021. As it can be noted, the AH sensors are highly reactive in recording the passage of the wave, and, also from this simple measurement, important considerations can be highlighted. In general, the evolution of water depth onto the field registered by each sensor is consistent with the expectation. More in detail, the water depth rapidly increases when the wavefront reaches the sensor; it remains approximately constant during the wetting phase and then decreases because of the combination of wavefront lateral dispersion and infiltration. On average, a decreasing trend of the maximum water depth is registered from the inlet point to the border ends. However, some singularities, typical of water propagation onto a tilted rough surface, are evidenced. For instance, the last two sensors (9 AH and 10 AH) measured higher water levels with respect to the one right before (8 AH). This is because there is an increase in surface roughness (detectable also from the terrain profile shown in Figure 9) that leads to a reduction of wavefront velocity and thus an increase in water depth (Takken and Govers, 2000). The same behaviour is evidenced in the 7 AH sensor concerning the 6 AH sensor as a result of the non-uniformity of surface roughness characteristics onto the field.

Figure 9 shows the evolution of the irrigation wavefront in the longitudinal direction. The free surface elevations were measured by the 10 AH sensors displaced along the agricultural field (Figure 4). It can be appreciated that, initially, the field starts to be gradually filled by the water (profiles 20 min, 30 min and 40 min in Figure 9), subsequently, there is a phase where the water levels remain almost stable along the agricultural field (profiles 50 min and 60 min in Figure 9) and finally, it begins to empty (profile 70 min in Figure 9) after the interruption of irrigation.

Data obtained from this experimental campaign by using AH devices as water level detectors could be employed to better understand border irrigation dynamics and in particular to describe both waterfront advance and recession, calculate the intake opportunity time, estimate uniformity of water distribution onto the field or calibrate hydrodynamical models (Costabile et al., 2023; Salahou et al., 2018).

Conclusions

We have presented a handmade low-cost sensor called ArduHydro to measure and monitor the water level in almost all situations where it is not possible to install fixed stations. The strengths of ArduHydro are: (i) the cost-effective (around 50 euros for a single sensor or around ~~35~~ 32 euros each for a batch of 10 sensors); (ii) based on the open-source Arduino technology, hence it is fully customizable to the user's needs in terms of sampling frequency rate and processing of the data; (iii) it is robust, compact, and easy to carry, therefore, suitable to work in extreme conditions; (iv) very precise when the distance from the free surface is around 50 cm or less, having an $R^2 > 0.91$ and a root-mean-square percentage error lower than 6% in comparison with the state-of-the-art laboratory ultrasonic sensors. This sensor can be used in many applications and here we have presented a possible one, i.e., the monitoring of water levels during border irrigation. Thanks to the ArduHydro sensor, it was possible to measure the advancement of the irrigation wavefront directly inside the field and hence collect important data to aid the modelling of surface irrigation dynamics. Differently from similar low-cost sensors based on Arduino technology present in the literature (e.g. Ezenne and Okoro, 2019; Hund et al., 2016; Kabi et al., 2023), ArduHydro sensors are particularly suitable for being used in large numbers to cover a relatively wide study area, to capture the dynamics of the phenomenon under consideration with high spatial coverage. This is especially useful in the agricultural context, where the control of water levels within the rural channel network or during irrigational overland flows is essential in the context of climate change in order to contrast water scarcity, an increasingly widespread problem in many Mediterranean areas (Braca et al., 2019; Peli et al., 2023).

References

Baden, T., Chagas, A.M., Gage, G., Marzullo, T., Prieto-Godino, L.L., Euler, T., 2015. Open Labware: 3-D Printing Your Own Lab Equipment. PLoS Biol 13, 1–12. https://doi.org/10.1371/journal.pbio.1002086

Braca, G., Bussettini, M., Ducci, D., Lastoria, B., Mariani, S., 2019. Evaluation of national and regional groundwater resources under climate change scenarios using a GIS-based water budget procedure. Rend Lincei Sci Fis Nat 30, 109–123. https://doi.org/10.1007/s12210-018-00757-6

Chen, B., Ouyang, Z., Sun, Z., Wu, L., Li, F., 2013. Evaluation on the potential of improving border irrigation performance through border dimensions optimization: A case study on the irrigation districts along the lower Yellow River. Irrig Sci 31, 715–728. https://doi.org/10.1007/s00271-012-0338-0

Cherqui, F., James, R., Poelsma, P., Burns, M.J., Szota, C., Fletcher, T., Bertrand-Krajewski, J.L., 2020. A platform and protocol to standardise the test and selection low-cost sensors for water level monitoring. H2Open Journal 3, 437–456. https://doi.org/10.2166/h2oj.2020.050

Chiaradia, E.A., Facchi, A., Masseroni, D., Ferrari, D., Bischetti, G.B., Gharsallah, O., Cesari de Maria, S., Rienzner, M., Naldi, E., Romani, M., Gandolfi, C., 2015. An integrated, multisensor system for the continuous monitoring of water dynamics in rice fields under different irrigation regimes. Environ Monit Assess 187. https://doi.org/10.1007/s10661-015-4796-8

Costabile, P., Costanzo, C., Gangi, F., De Gaetani, C.I., Rossi, L., Gandolfi, C., Masseroni, D., 2023. High-resolution 2D modelling for simulating and improving the management of border irrigation. Agric Water Manag 275. https://doi.org/10.1016/j.agwat.2022.108042

Dawson, C.W., Abrahart, R.J., See, L.M., 2007. HydroTest: A web-based toolbox of evaluation metrics for the standardised assessment of hydrological forecasts. Environ Model Softw 22, 1034–1052. https://doi.org/10.1016/j.envsoft.2006.06.008

Errico, A., Lama, G.F.C., Francalanci, S., Chirico, G.B., Solari, L., Preti, F., 2019. Flow dynamics and turbulence patterns in a drainage channel colonized by common reed (Phragmites australis) under different scenarios of vegetation management. Ecol Eng 133, 39–52. https://doi.org/10.1016/j.ecoleng.2019.04.016

Ezenne, G.I., Okoro, G.O., 2019. Development of a low-cost automatic water level monitoring system. Agricultural Engineering International: CIGR Journal 21, 1–6.

Facchi, A., Masseroni, D., Miniotti, E.F., 2017. Self-made microlysimeters to measure soil evaporation: a test on aerobic rice in northern Italy. Paddy Water Environ 15, 669–680. https://doi.org/10.1007/s10333-016-0566-7

Fisher, D.K., Fletcher, R.S., Anapalli, S.S., 2020. Evolving Open-Source Technologies Offer Options for Remote Sensing and Monitoring in Agriculture. Advances in Internet of Things 10, 1–10. https://doi.org/10.4236/ait.2020.101001

Fisher, D.K., Gould, P.J., 2012. Open-Source Hardware Is a Low-Cost Alternative for Scientific Instrumentation and Research. Modern Instrumentation 01, 8–20. https://doi.org/10.4236/mi.2012.12002

Gao, A., Wu, S., Wang, F., Wu, X., Xu, P., Yu, L., Zhu, S., 2019. A newly developed unmanned aerial vehicle (UAV) imagery based technology for field measurement of water level. Water 11. https://doi.org/10.3390/w11010124

Harnett, C., 2011. Open source hardware for instrumentation and measurement. IEEE Instrum Meas Mag 14, 34–38. https://doi.org/10.1109/MIM.2011.5773535

Herschy, R.W., 2009. Streamflow Measurement, 3rd ed. Taylor & Francis, New York, USA.

Hilsenrath, J., Beckett, C.W., William, S.B., Fano, L., Hoge, H.J., Masi, J.F., Nuttall, R.L., Touloukian, Y.S., Woolley, H.W., 1955. Tables of Thermal Properties of Gases, Circular 5. ed. US Department of Commerce, National Bureau of Standards.

Hund, S. V., Johnson, M.S., Keddie, T., 2016. Developing a Hydrologic Monitoring Network in Data-Scarce Regions Using Open-Source Arduino Dataloggers. Agric Environ Lett 1, 160011. https://doi.org/10.2134/ael2016.02.0011

Ichikawa, K., Ebinuma, T., Konda, M., Yufu, K., 2019. Low-cost GNSS-R altimetry on a UAV for water-level measurements at arbitrary times and locations. Sensors 19. https://doi.org/10.3390/s19050998

Illes, C., Popa, G.N., Filip, I., 2013. Water level control system using PLC and wireless sensors. ICCC 2013 - IEEE 9th International Conference on Computational Cybernetics, Proceedings 195–199. https://doi.org/10.1109/ICCCyb.2013.6617587

Kabi, J.N., wa Maina, C., Mharakurwa, E.T., Mathenge, S.W., 2023. Low cost, LoRa based river water level data acquisition system. HardwareX e00414. https://doi.org/10.1016/j.ohx.2023.e00414

Karegar, M.A., Kusche, J., Geremia-Nievinski, F., Larson, K.M., 2022. Raspberry Pi Reflector (RPR): A Low-Cost Water-Level Monitoring System Based on GNSS Interferometric Reflectometry. Water Resour Res 58. https://doi.org/10.1029/2021WR031713

Loizou, K., Koutroulis, E., 2016. Water level sensing: State of the art review and performance evaluation of a low-cost measurement system. Measurement 89, 204–214. https://doi.org/10.1016/j.measurement.2016.04.019

Loizou, K., Koutroulis, E., Zalikas, D., Liontas, G., 2015. A low-cost sensor based on time-domain reflectometry for water level monitoring in environmental applications. 2015 IEEE 15th International Conference on Environment and Electrical Engineering, EEEIC 2015 - Conference Proceedings 261–266. https://doi.org/10.1109/EEEIC.2015.7165549

Mao, F., Khamis, K., Krause, S., Clark, J., Hannah, D.M., 2019. Low-Cost Environmental Sensor Networks: Recent Advances and Future Directions. Front Earth Sci 7, 1–7. https://doi.org/10.3389/feart.2019.00221

Marino, M., Rabionet, I.C., Musumeci, R.E., Foti, E., 2018. Reliability of Pressure Sensors To Measure Wave Height in the Shoaling Region. Proceedings of the 36th International Conference on Coastal Engineering 10. https://doi.org/10.9753/icce.v36.papers.10

Masseroni, D., Castagna, A., Gandolfi, C., 2021. Evaluating the performances of a flexible mechanism of water diversion: application on a northern Italy gravity-driven irrigation channel. Irrig Sci 39, 363–373. https://doi.org/10.1007/s00271-020-00718-8

Masseroni, D., Facchi, A., Depoli, E.V., Renga, F.M., Gandolfi, C., 2016. Irrig-OH: An Open-Hardware Device for Soil Water Potential Monitoring and Irrigation Management. Irrig Drain 65, 750–761. https://doi.org/10.1002/ird.1989

Masseroni, D., Gangi, F., Galli, A., Ceriani, R., De Gaetani, C., Gandolfi, C., 2022. Behind the efficiency of border irrigation: Lesson learned in Northern Italy. Agric Water Manag 269, 107717. https://doi.org/10.1016/j.agwat.2022.107717

Masseroni, D., Ricart, S., de Cartagena, F.R., Monserrat, J., Gonçalves, J.M., de Lima, I., Facchi, A., Sali, G., Gandolfi, C., 2017. Prospects for improving gravity-fed surface irrigation systems in mediterranean european contexts. Water 9. https://doi.org/10.3390/w9010020

Montanari, A., Young, G., Savenije, H.H.G., Hughes, D., Wagener, T., Ren, L.L., Koutsoyiannis, D., Cudennec, C., Toth, E., Grimaldi, S., Blöschl, G., Sivapalan, M., Beven, K., Gupta, H., Hipsey, M., Schaefli, B., Arheimer, B., Boegh, E., Schymanski, S.J., Di Baldassarre, G., Yu, B., Hubert, P., Huang, Y., Schumann, A., Post, D.A., Srinivasan, V., Harman, C., Thompson, S., Rogger, M., Viglione, A., McMillan, H., Characklis, G., Pang, Z., Belyaev, V., 2013. "Panta Rhei-Everything Flows": Change in hydrology and society-The IAHS Scientific Decade 2013-2022. Hydrol Sci J 58, 1256–1275. https://doi.org/10.1080/02626667.2013.809088

Noto, S., Tauro, F., Petroselli, A., Apollonio, C., Botter, G., Grimaldi, S., 2021. Technical Note: Low cost stage-camera system for continuous water level monitoring in ephemeral streams. Hydrol Earth Syst Sci Discuss 1–17. https://doi.org/10.5194/hess-2021-36

Pearce, J.M., 2012. Building research equipment with free, open-source hardware. Science (1979) 337, 1303–1304. https://doi.org/10.1126/science.1228183

Peli, M., Rapuzzi, C., Barontini, S., Ranzi, R., 2023. Application of Benfratello's method to estimate the spatio-temporal variability of the irrigation deficit in a Mediterranean semiarid climate. Hydrol Res. https://doi.org/10.2166/nh.2023.081

Persi, E., Petaccia, G., Fenocchi, A., Manenti, S., Ghilardi, P., Sibilla, S., 2019. Hydrodynamic coefficients of yawed cylinders in open-channel flow. Flow Meas Instrum 65, 288–296. https://doi.org/10.1016/j.flowmeasinst.2019.01.006

Peruzzi, C., Galli, A., Chiaradia, E.A., Masseroni, D., 2021a. Evaluating longitudinal dispersion of scalars in rural channels of agro-urban environments. Environ Fluid Mech 21, 925–954. https://doi.org/10.1007/s10652-021-09804-7

Peruzzi, C., Poggi, D., Ridolfi, L., Manes, C., 2020. On the scaling of large-scale structures in smooth-bed turbulent open-channel flows. J Fluid Mech 889. https://doi.org/10.1017/jfm.2020.73

Peruzzi, C., Vettori, D., Poggi, D., Blondeaux, P., Ridolfi, L., Manes, C., 2021b. On the influence of collinear surface waves on turbulence in smooth-bed open-channel flows. J Fluid Mech 924, 1–37. https://doi.org/10.1017/jfm.2021.605

Purnell, D.J., Gomez, N., Minarik, W., Porter, D., Langston, G., 2021. Precise water level measurements using low-cost GNSS antenna arrays. Earth Surf Dyn 9, 673–685. https://doi.org/10.5194/esurf-9-673-2021

Ravazzani, G., 2017. Open hardware portable dual-probe heat-pulse sensor for measuring soil thermal properties and water content. Comput Electron Agric 133, 9–14. https://doi.org/10.1016/j.compag.2016.12.012

Rosolem, J.B., Dini, D.C., Penze, R.S., Floridia, C., Leonardi, A.A., Loichate, M.D., Durelli, A.S., 2013. Fiber optic bending sensor for water level monitoring: Development and field test: A review. IEEE Sens J 13, 4113–4120. https://doi.org/10.1109/JSEN.2013.2278074

Salahou, M.K., Jiao, X., Lü, H., 2018. Border irrigation performance with distance-based cut-off. Agric Water Manag 201, 27–37. https://doi.org/10.1016/j.agwat.2018.01.014

Schoener, G., 2018. Time-Lapse Photography: Low-Cost, Low-Tech Alternative for Monitoring Flow Depth. J Hydrol Eng 23, 06017007. https://doi.org/10.1061/(asce)he.1943-5584.0001616

Shen, J., 1981. Discharge Characteristics of Triangular-Notch Thin-Plate Weirs., US Geological Survey Water Supply Paper. https://doi.org/10.3133/wsp1617B

Takken, I., Govers, G., 2000. Hydraulics of interrill overland flow on rough, bare soil surfaces. Earth Surf Process Landf 25, 1387–1402. https://doi.org/10.1002/1096-9837(200012)25:13<1387::AID-ESP135>3.0.CO;2-D

Tauro, F., Selker, J., Van De Giesen, N., Abrate, T., Uijlenhoet, R., Porfiri, M., Manfreda, S., Caylor, K., Moramarco, T., Benveniste, J., Ciraolo, G., Estes, L., Domeneghetti, A., Perks, M.T., Corbari, C., Rabiei, E., Ravazzani, G., Bogena, H., Harfouche, A., Broccai, L., Maltese, A., Wickert, A., Tarpanelli, A., Good, S., Lopez Alcala, J.M., Petroselli, A., Cudennec, C., Blume, T., Hut, R., Grimaldia, S., 2018. Measurements and observations in the XXI century (MOXXI): Innovation and multi-disciplinarity to sense the hydrological cycle. Hydrol Sci J 63, 169–196. https://doi.org/10.1080/02626667.2017.1420191

Toran, L., 2016. Water level loggers as a low-cost tool for monitoring of stormwater control measures. Water 8. https://doi.org/10.3390/w8080346

Tscheikner-Gratl, F., Caradot, N., Cherqui, F., Leitão, J.P., Ahmadi, M., Langeveld, J.G., Le Gat, Y., Scholten, L., Roghani, B., Rodríguez, J.P., Lepot, M., Stegeman, B., Heinrichsen, A., Kropp, I., Kerres, K., Almeida, M. do C., Bach, P.M., Moy de Vitry, M., Sá Marques, A., Simões, N.E., Rouault, P., Hernandez, N., Torres, A., Werey, C., Rulleau, B., Clemens, F., 2019. Sewer asset management–state of the art and research needs. Urban Water J 16, 662–675. https://doi.org/10.1080/1573062X.2020.1713382

Vijay Hari Ram, V., Vishal, H., Dhanalakshmi, S., Meenakshi Vidya, P., 2015. Regulation of water in agriculture field using Internet Of Things. Proceedings - 2015 IEEE International Conference on Technological Innovations in ICT for Agriculture and Rural Development, TIAR 2015 112–115. https://doi.org/10.1109/TIAR.2015.7358541

Wickert, A.D., Sandell, C.T., Schulz, B., Ng, G.H.C., 2019. Open-source Arduino-compatible data loggers designed for field research. Hydrol Earth Syst Sci 23, 2065–2076. https://doi.org/10.5194/hess-23-2065-2019

Wong, G.S.K., Embleton, T.F., 1985. Variation of the speed of sound in air with humidity and temperature. J Acoust Soc Am 77, 1710–1712. https://doi.org/10.1121/1.391918

Zhang, G., Valero, D., Bung, D.B., Chanson, H., 2018. On the estimation of free-surface turbulence using ultrasonic sensors. Flow Meas Instrum 60, 171–184. https://doi.org/10.1016/j.flowmeasinst.2018.02.009

Zhang, Z., Zhou, Y., Liu, H., Gao, H., 2019. In-situ water level measurement using NIR-imaging video camera. Flow Meas Instrum 67, 95–106. https://doi.org/10.1016/j.flowmeasinst.2019.04.004
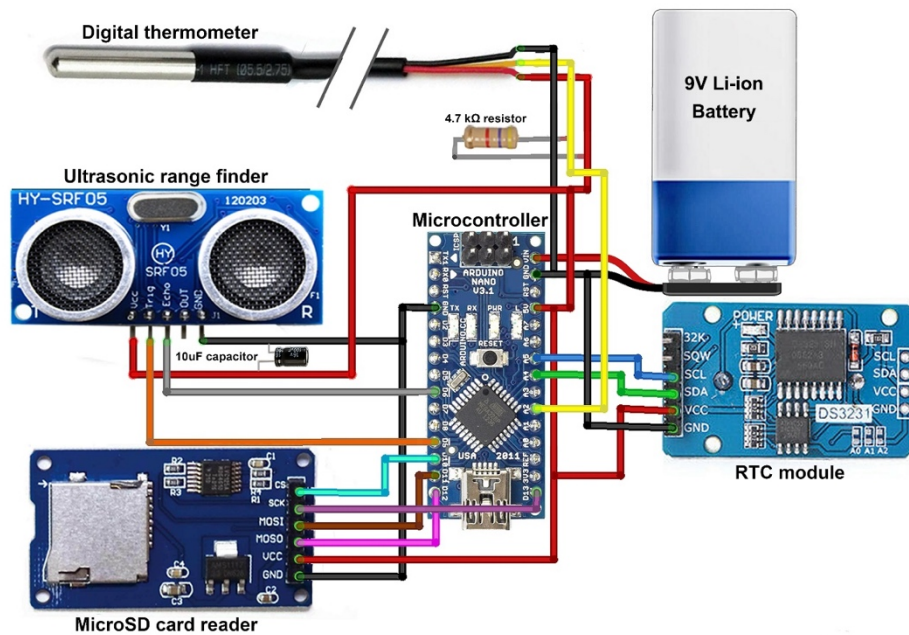
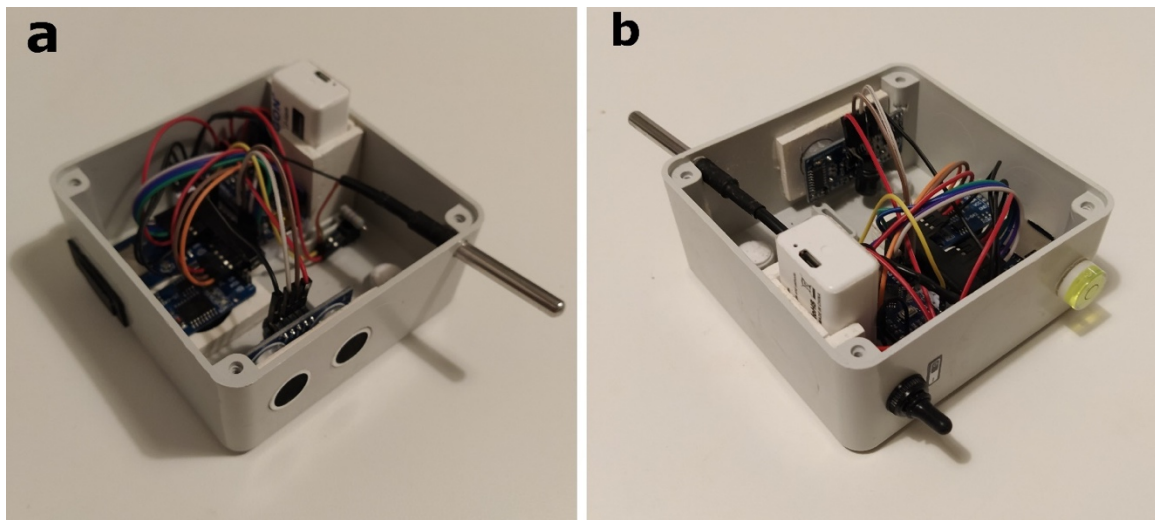**Figure 1. Wiring diagram of ArduHydro components.**

Figure 2. Inside view of ArduHydro; (a) lower part with sensors; (b) upper part with switch and bubble level.
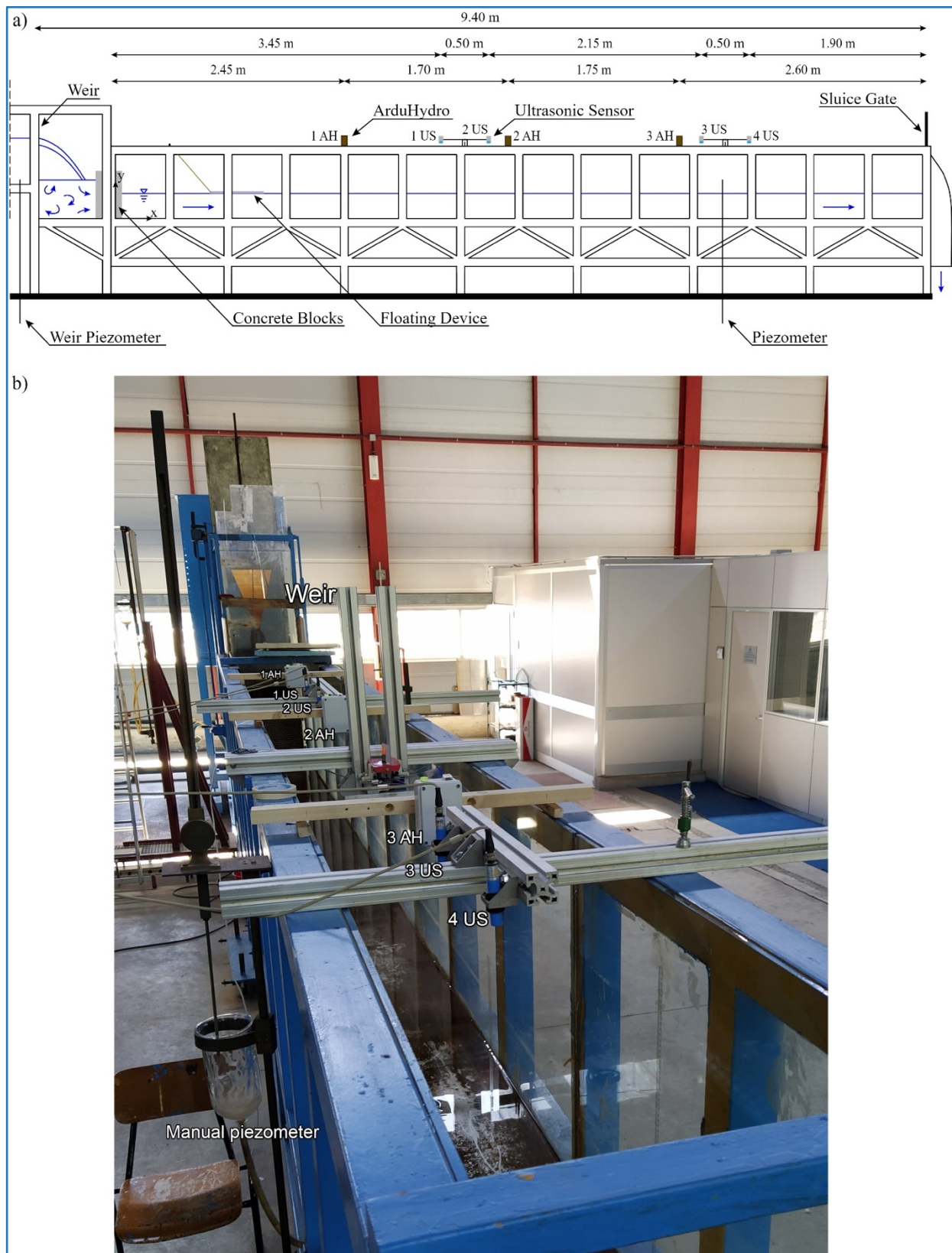
Figure 3. a) Sketch of the whole hydraulic circuit used in the experiments (adapted from Persi et al., 2019); b) photo of the open-channel flume facility with the installed sensors (AH=ArduHydro sensor; US=ultrasonic sensor).
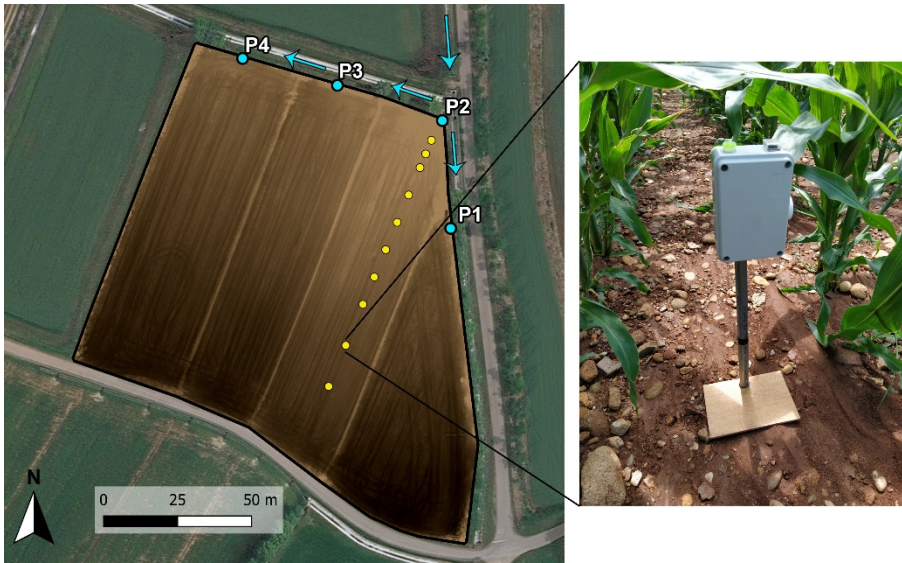
Figure 4. The agricultural field with the indication of the four sectors. The blue points indicate the water inlet whereas the yellow points represent the ArduHydro positions within the second sector. The enlargement on the right shows an on-field installation of an ArduHydro sensor.
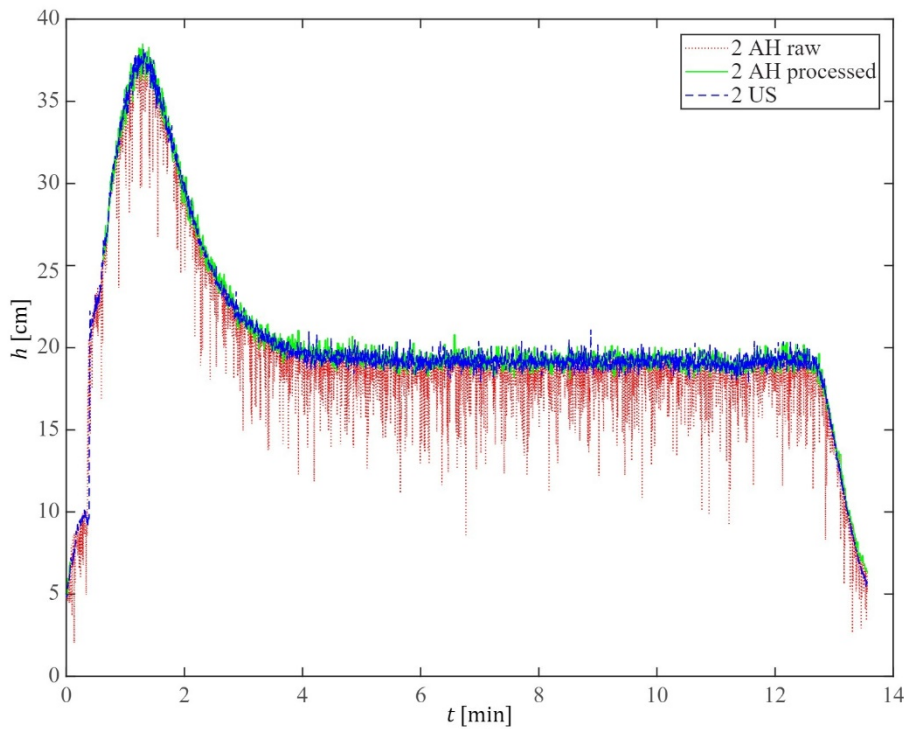

Figure 5. Data filtering results. Raw AH data are shown in red, while processed data and US data are shown in green and blue, respectively.
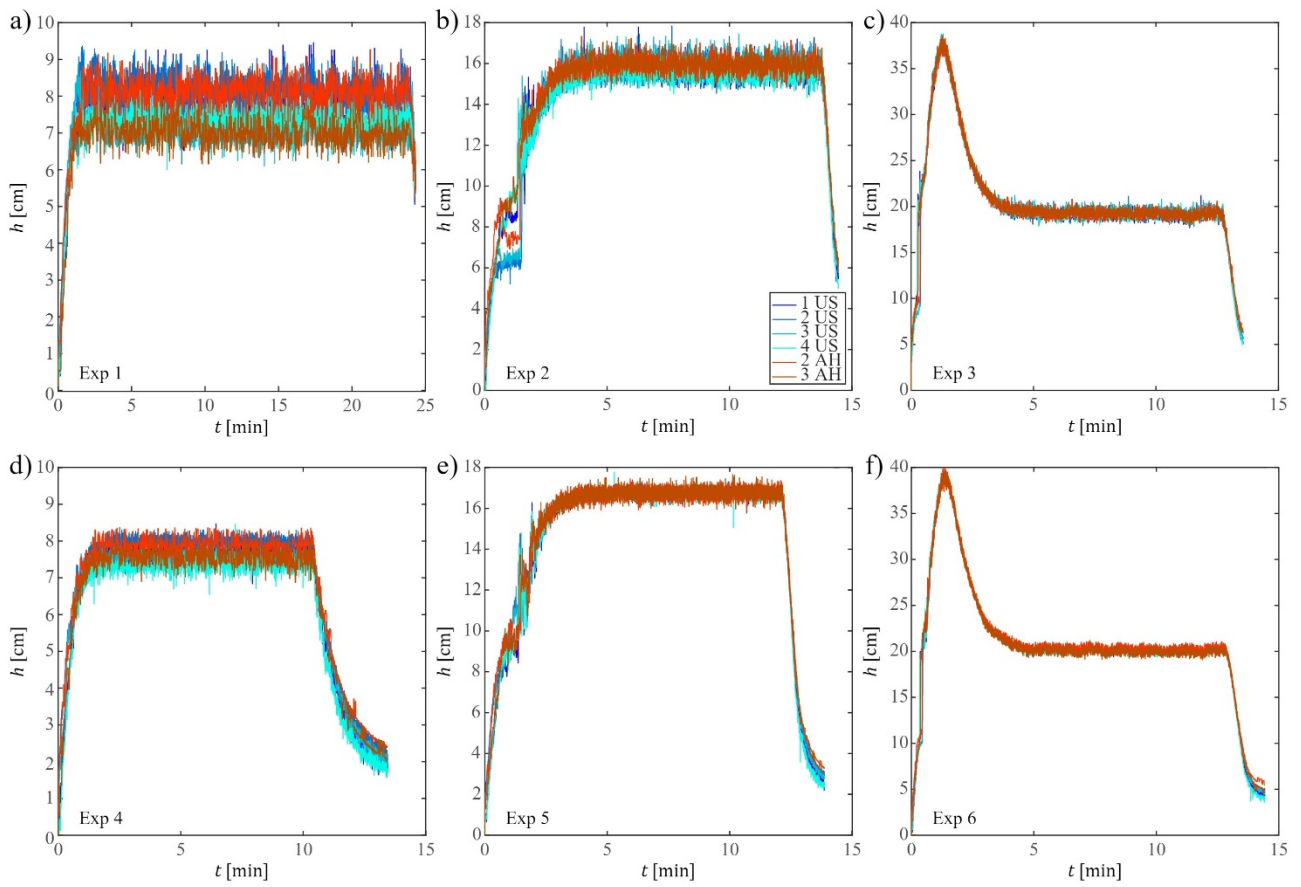
Figure 6. Free surface profiles for each experiment. The water levels measured by the 1 AH sensor are not reported for clarity purposes.

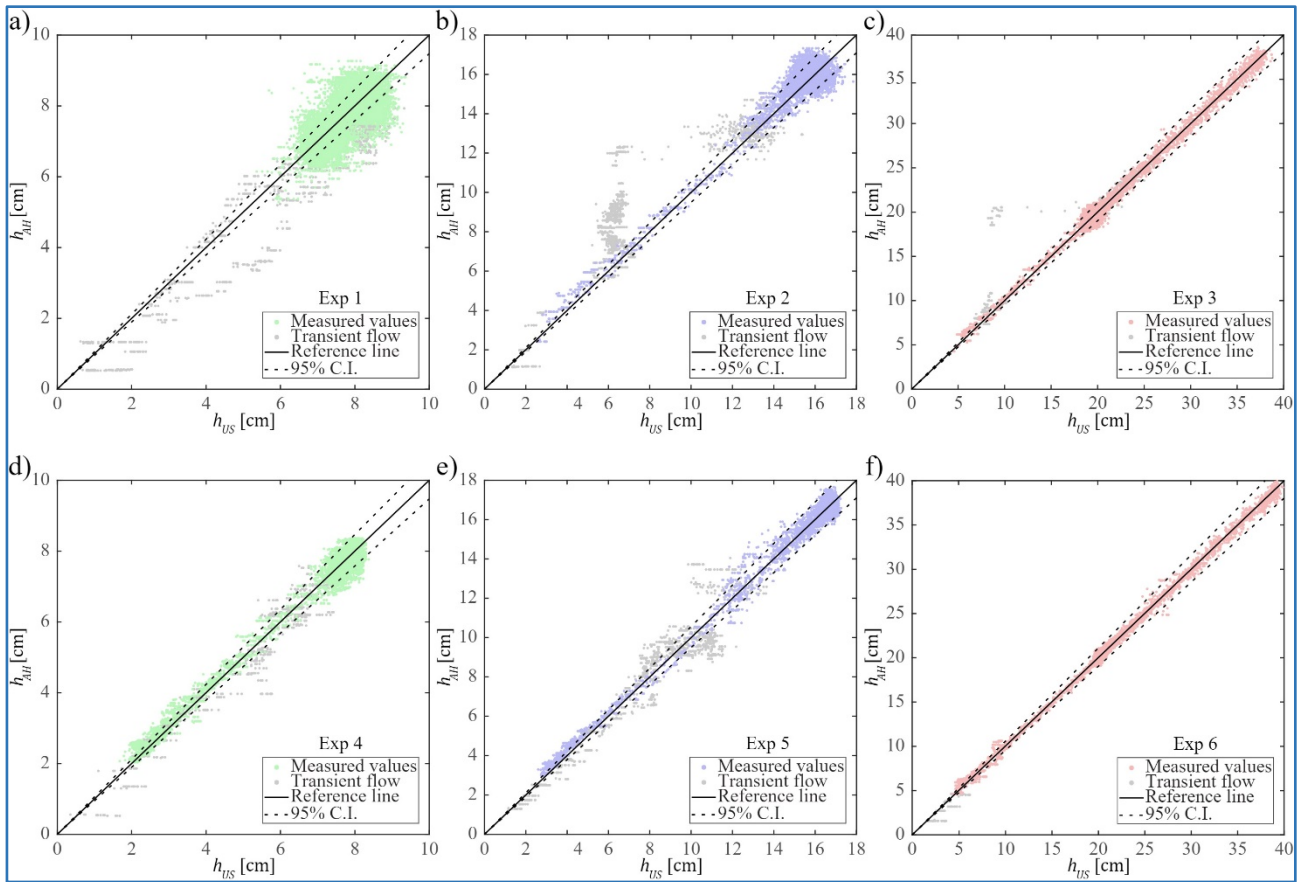**Figure 7. Scatter plot reporting the water levels measured by ~~the AH sensors (h_{AH})~~ the US sensors (h_{US}) versus the water level measured by ~~the US sensors (h_{US})~~ the AH sensors (h_{AH}). Each panel reports the water levels measured both in ~~the~~ positions 2 and 3 in the flume (Figure 3a). All the panels also display the data measured during the passage of the transient flow (grey dots).**

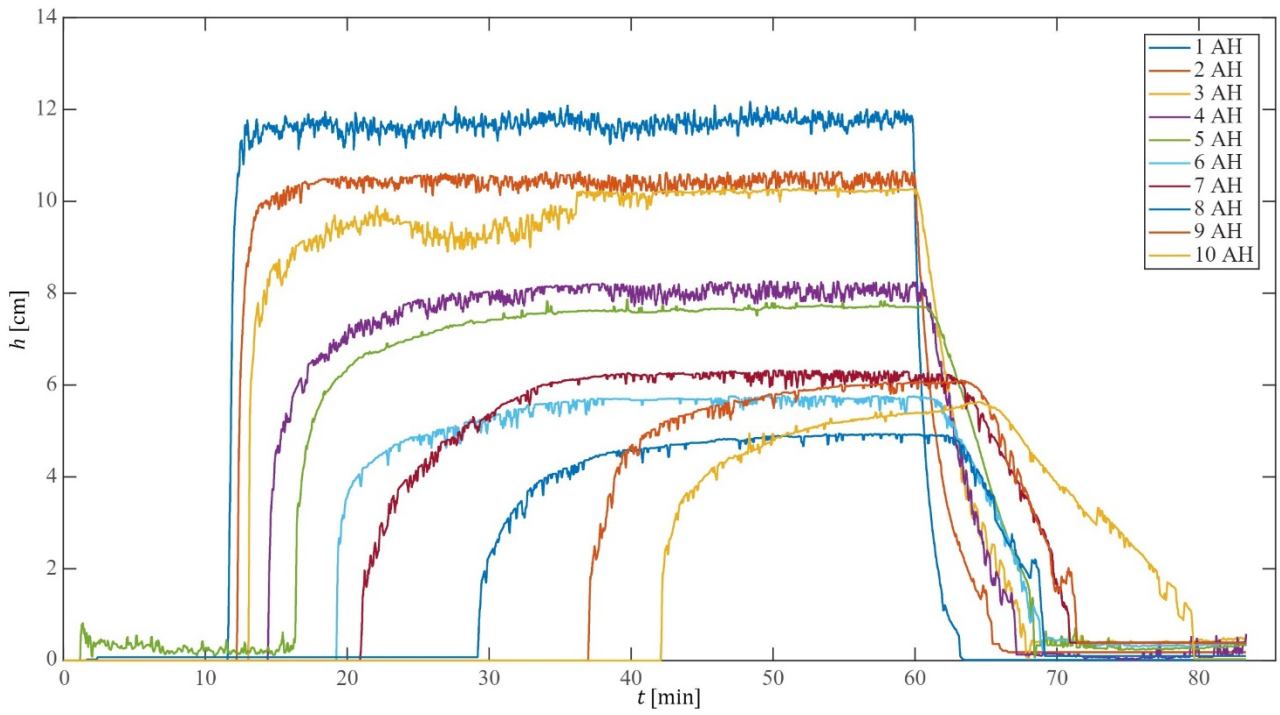**Figure 8. Evolution of the irrigational wavefront captured by the 10 AH sensors displaced along the sector.**
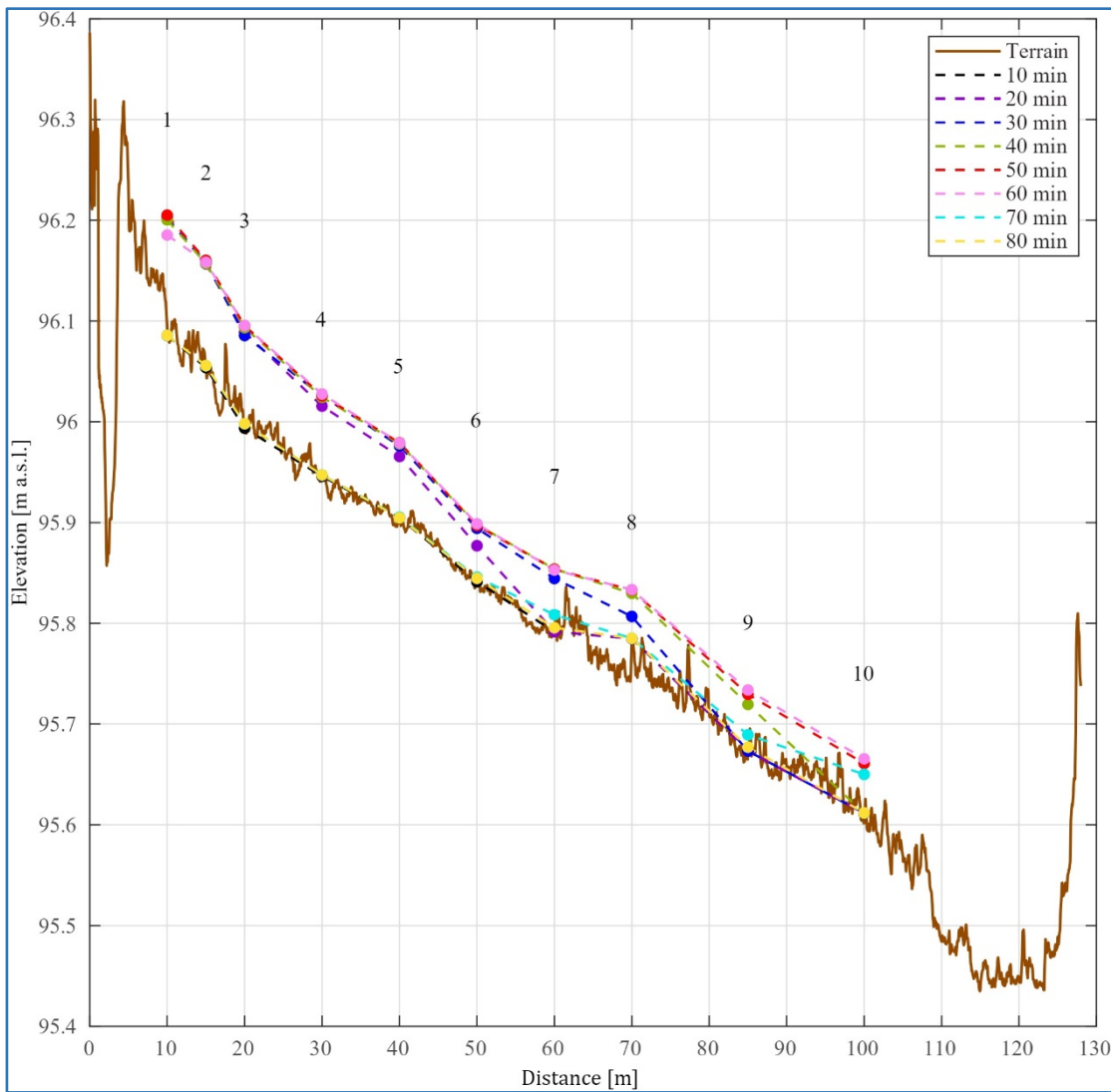
Figure 9. Longitudinal profiles of the free surface elevation. The profiles were extracted at regular intervals of 10 minutes each during the irrigation event along the longitudinal direction of the field. The colored-filled circles are associated with the position of the AH sensors (Figure 4).

Table 1. List of ArduHydro components (updated to October 2022 prices updated to July 2023).

Name	Function	Supplier	Cost (€)	Batch cost (€)
Nano V3.0 CH340	Microcontroller	Az-Delivery	~~9.99~~ 11.49	~~6.99~~ 6.19
HY-SRF05	Ultrasonic sensor	HitLetGo	7.99	4.33
DS18B20	Temperature sensor	Az-Delivery	~~5.99~~ 2.99	~~3.39~~ 1.59
RTC DS3231	RTC Module	Az-Delivery	~~7.99~~ 6.99	~~4.59~~ 2.99
MicroSD Card Adapter	MicroSD reader	Az-Delivery	3.99	~~1.89~~ 1.29
9V Li-ion rechargeable battery	Battery	ENEGON	10.50	9.49
Other components	Various	Local hardware stores	5.90	5.90
Total			~~52.35~~ 49.85	~~36.58~~ 31.78

Table 2. Summary of experiments and associated hydraulic conditions. Q is the flow rate; h_p is the water depth measured by the downstream manual piezometer after the setting of the steady-state conditions; $U_b = Q/Wh_p$ is the bulk velocity estimated after the setting of the steady-state conditions, where W is the channel width, and $Fr = U_b/\sqrt{g\,h_p}$ is the Froude number, where g is the gravitational acceleration.

Run	Q [l/s]	h_p [cm]	U_b [cm/s]	Fr [-]	Duration	Floating Device
Exp 1	23.82	6.9	~~26.1~~ 70.4	~~0.32~~ 0.85	24 min 26 sec	No
Exp 2	36.76	15.2	~~27.7~~ 49.3	~~0.23~~ 0.40	14 min 03 sec	No
Exp 3	40.70	18.6	~~27.3~~ 44.6	~~0.20~~ 0.33	13 min 05 sec	No
Exp 4	23.65	6.8	~~26.0~~ 71.0	~~0.32~~ 0.87	23 min 10 sec	Yes
Exp 5	37.31	16.3	~~27.1~~ 46.7	~~0.21~~ 0.37	12 min 20 sec	Yes
Exp 6	41.06	19.5	~~26.8~~ 43.0	~~0.19~~ 0.31	10 min 58 sec	Yes

Table 3. Arrangement information of the AH sensors reported in Figure 4 for the irrigation event of July 20, 2021.

# of AH sensor	Distance from the previous AH sensor [m]	Progressive distance from the inlet [m]	Elevation from the ground [cm]
1	0	10	30.8
2	5	15	31.9
3	5	20	32.8
4	5	30	36.2
5	10	40	33.4
6	10	50	28.0
7	10	60	33.5
8	10	70	29.0
9	15	85	31.5
10	15	100	30.5

Table 4. Pearson correlation coefficient r, coefficient of determination R^2, and root-mean-square error $RMSE$ for the two investigated positions.

	Comparison 2 AH – 2 US			Comparison 3 AH – 3 US		
	r [-]	R^2 [-]	$RMSE$ [cm]	r [-]	R^2 [-]	$RMSE$ [cm]
Exp 1	0.835	0.669	0.540	0.820	0.504	0.532
Exp 2	0.974	0.930	0.874	0.962	0.915	0.959
Exp 3	0.994	0.987	0.643	0.985	0.969	0.999
Exp 4	0.990	0.978	0.294	0.989	0.977	0.289
Exp 5	0.994	0.989	0.451	0.993	0.987	0.495
Exp 6	0.997	0.993	0.564	0.994	0.988	0.752